Acta Pharmaceutica Sinica B 2020;10(12):2404–2416

Chinese Pharmaceutical Association
Institute of Materia Medica, Chinese Academy of Medical Sciences

Acta Pharmaceutica Sinica B

www.elsevier.com/locate/apsb
www.sciencedirect.com

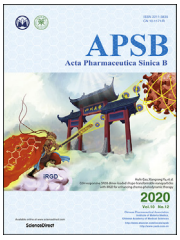

ORIGINAL ARTICLE

A homogenous nanoporous pulmonary drug delivery system based on metal-organic frameworks with fine aerosolization performance and good compatibility

Yixian Zhou[a,†], Boyi Niu[a,†], Biyuan Wu[a], Sulan Luo[a], Jintao Fu[a], Yiting Zhao[a], Guilan Quan[b,*], Xin Pan[a], Chuanbin Wu[a,*]

[a]*School of Pharmaceutical Sciences, Sun Yat-sen University, Guangzhou 510006, China*
[b]*College of Pharmacy, Jinan University, Guangzhou 510632, China*

Received 13 March 2020; received in revised form 24 May 2020; accepted 19 June 2020

KEY WORDS

Pulmonary drug delivery;
Metal-organic framework;
Inhalable dry powder;
Nanoporous particle

Abstract Pulmonary drug delivery has attracted increasing attention in biomedicine, and porous particles can effectively enhance the aerosolization performance and bioavailability of drugs. However, the existing methods for preparing porous particles using porogens have several drawbacks, such as the inhomogeneous and uncontrollable pores, drug leakage, and high risk of fragmentation. In this study, a series of cyclodextrin-based metal-organic framework (CD-MOF) particles containing homogenous nanopores were delicately engineered without porogens. Compared with commercial inhalation carrier, CD-MOF showed excellent aerosolization performance because of the homogenous nanoporous structure. The great biocompatibility of CD-MOF in pulmonary delivery was also confirmed by a series of experiments, including cytotoxicity assay, hemolysis ratio test, lung function evaluation, *in vivo* lung injury markers measurement, and histological analysis. The results of *ex vivo* fluorescence imaging showed

Abbreviations: γ-CD, γ-cyclodextrin; ANOVA, analysis of variance; BALF, bronchoalveolar lavage fluid; BET, Brunauer–Emmett–Teller; CCK-8, cell counting kit-8; CD-MOF, cyclodextrin-based metal-organic framework; CD-MOF-K, ketoprofen-loaded cyclodextrin-based metal-organic framework; CD-MOF-R, rhodamine B-loaded cyclodextrin-based metal-organic framework; C_{dyn}, dynamic lung compliance; CF, commercial formulation; CTAB, cetyl trimethyl ammonium bromide; DPPC, 1,2-dipalmitoyl-*sn*-glycero-3-phosphocholine; FBS, fetal bovine serum; FDA, U.S. Food and Drug Administration; FPF, fine particle fraction; GSD, geometric standard deviation; HE, Hematoxylin-Eosin; HPLC, high performance liquid chromatography; LDH, lactate dehydrogenase; LPS, lipopolysaccharide; MFI, mean fluorescence intensity; MMAD, mean mass aerodynamic diameter; MOF, metal-organic framework; NGI, next generation pharmaceutical impactor; PBS, phosphate buffered solution; PVP, poly(vinyl pyrrolidone); PXRD, powder X-ray diffraction; R_l, lung resistance; SD rat, Sprague–Dawley rat; SEM, scanning electron microscopy; SLF, simulated lung fluid.

*Corresponding authors.
E-mail addresses: xiaoplanet@163.com (Guilan Quan), wuchuanb@mail.sysu.edu.cn (Chuanbin Wu).
†These authors made equal contributions to this work.

Peer review under responsibility of Chinese Pharmaceutical Association and Institute of Materia Medica, Chinese Academy of Medical Sciences.

https://doi.org/10.1016/j.apsb.2020.07.018

the high deposition rate of CD-MOF in lungs. Therefore, all results demonstrated that CD-MOF was a promising carrier for pulmonary drug delivery. This study may throw light on the nanoporous particles for effective pulmonary administration.

1. Introduction

Pulmonary drug delivery has attracted great interest in recent years, owing to its numerous advantages over the injection and oral administration. Specifically, pulmonary drug delivery systems can not only directly deliver therapeutic agents to lungs with high efficiency for local diseases including respiratory diseases and lung cancer[1], but also significantly promote the drug absorption for systematic diseases. This is due to the special physiological characteristics of lungs, including large alveolar surface (~100 m^2), thin alveolar epithelium (~0.2 μm), extensive vascularization, and low enzymatic metabolic activity[2–4]. Moreover, the pulmonary administration can avoid first pass metabolism caused by oral administration and decrease pain and discomfort of patients associated with injection[5].

Lung deposition rate, the prerequisite for pulmonary drug delivery, has direct impact on the therapeutic effects, which is closely related to the aerosolization performance of inhaled particles. The aerosolization performance is mainly affected by the size distribution and the structure of particles[6,7]. Generally, particles with size range between 1 and 5 μm are appropriate for deep lung deposition[1,8]. Moreover, the particles with porous structure are favorable for improving the aerosolization efficiency because of the remarkably reduced density and small aerodynamic diameter[9,10]. There are many methods for preparing porous particles, such as single emulsion method[11], multiple emulsion method[10], spray drying method[12], and supercritical fluids method[13]. Porogens are commonly used during the preparation process, such as ammonium bicarbonate[14], poly(vinyl pyrrolidone) (PVP)[11], and Pluronic F127[15]. However, the addition of porogens may bring some inevitable drawbacks. First, the pores generated by porogens are often inhomogeneous and uncontrollable, which may cause variability between inter- and intra-batches[16]. Second, the porogens are commonly removed by high temperature or leaching with solvents. During those processes, the encapsulated drugs may be degraded by heating or removed away by solvents[17]. Third, the pores produced by porogens are often macropores (more than 50 nm), which may increase friability and risk of fragmentation for particles. Therefore, developing porous system without using porogens is a promising strategy for pulmonary drug delivery. Although some porous systems, such as mesoporous silica particles, have been used for pulmonary administration[18], their poor biocompatibility seriously impeded further applications[19]. It is necessary to develop a novel porous system with good biocompatibility.

Metal-organic frameworks (MOFs) are a new class of porous materials composed of metal ions and organic linkers, which have been extensively studied for versatile applications in various fields, such as catalysis, separation, sensing, and gas storage[20–28]. Besides applications in these fields, the unique advantages including high porosity, large surface area, and excellent flexibility make MOFs suitable carriers for drug delivery[29–32]. The pores of MOFs are formed because of their periodic network structures, which are self-assembled by coordination bonding between metal ions and organic links without using any porogens. Moreover, the pores of MOFs ranged in nanoscale with strict homogeneity, which are usually less than 2 nm. Therefore, MOFs may be promising candidates in pulmonary administration. However, the excipients for pulmonary drug delivery approved by U.S. Food and Drug Administration (FDA) are very limited, and the toxicity of MOFs may add uncertainty to its further development[33]. The safety of the carrier in pulmonary administration has to undergo stringent assessment.

Cyclodextrin-based metal-organic framework (CD-MOF) is a type of MOFs with great biocompatibility, which is composed of potassium ions and γ-cyclodextrin[34,35]. CD-MOF is body-centered cubic structure containing apertures of 7.8 Å and large spherical pores of 17 Å in diameter[36,37]. Drug molecules containing carboxyl or hydroxyl groups in suitable size can be loaded into the cavity of CD-MOF through electrostatic interactions and hydrogen bonds[38]. We hypothesized that CD-MOF was a potential vehicle for pulmonary drug delivery for the follow reasons. (i) The homogenous nanoscale pores of CD-MOF could effectively improve the aerosolization performance. (ii) The particle size of CD-MOF could be delicately engineered by changing the reaction factors during synthesis[37] to achieve higher lung deposition efficiency. (iii) The biocompatibility of CD-MOF was good since cyclodextrin, the organic linker of CD-MOF, was widely used as an excipient in pulmonary drug delivery, which was proven to be safe[39–41]. (iv) The synthesis was facile and could be finished in one step.

In this study, a series of CD-MOFs with various size distribution was synthesized *via* a vapor diffusion method. The model drug ketoprofen, which can effectively fight pulmonary inflammation by topical delivery[42,43], was loaded into CD-MOF by a co-crystallisation method during the synthetic process in one step. The physicochemical properties and aerodynamic performance of the particles were characterized. In order to prove the potential of CD-MOF in pulmonary delivery, a series of experiments including cytotoxicity assay, hemolysis ratio test, lung function evaluation, *in vivo* lung injury markers measurement, and histological analysis were performed. Moreover, *ex vivo* fluorescence imaging was carried out to further investigate the *in vivo* fate of drug delivery system.

2. Materials and methods

2.1. Materials

Cetyl trimethyl ammonium bromide (CTAB), ketoprofen, and lipopolysaccharide (LPS) were purchased from Aladdin Industrial Ltd. (Shanghai, China). γ-Cyclodextrin (γ-CD) was supplied by MaxDragon Biochemical Ltd. (Guangzhou, China). Potassium hydroxide (KOH) was purchased from Shanghai Macklin Biochemical Ltd. (Shanghai, China). InhaLac® 230 was

purchased from Meggle Ltd. (Wasserburg, Germany). 1,2-Dipalmitoyl-*sn*-glycero-3-phosphocholine (DPPC) was supplied by Corden Pharma Switzerland LLC (Liestal, Switzerland). DMEM, RPMI 1640 medium, penicillin and streptomycin solution, and 0.25% trypsin solution were obtained from Gibco Life Technology Ltd. (Waltham, USA). Fetal bovine serum (FBS) was purchased from Thermo Fisher Scientific Inc. (Waltham, USA). Ethanol, methanol, and isopropanol were supplied by Tianjin Zhiyuan Chemical Reagent Ltd. (Tianjin, China).

2.2. Cells and animals

A549 and Calu-3 cells were cultured in DMEM and RPMI 1640 medium, respectively. The culture medium was supplemented with 10% FBS (*v*/*v*) and 1% penicillin and streptomycin (*v*/*v*). All cells were cultured in an incubator containing 5% CO_2 at 37 °C.

The healthy Sprague−Dawley (SD) rats were purchased from Beijing Vital River Laboratory Animal Technology Co., Ltd. (Beijing, China). All animal experiments were carried out in accordance with the guiding principles for the care and use of laboratory animals approved by the Institutional Animal Care and Ethics Committee, Sun Yat-sen University (Guangzhou, China; Approval No.: SYSU-IACUC-2019-000085).

2.3. Synthesis of CD-MOF and ketoprofen-loaded CD-MOF (CD-MOF-K)

γ-CD and KOH were dissolved in deionized water at a concentration of 32.4 and 11.2 mg/mL, respectively. The obtained solution was filtered through a 0.8 μm filter, followed by adding a defined amount of methanol. After incubation in water bath at 50 °C, CTAB and methanol were added into the solution under violent stirring. The mixed solution was incubated at room temperature. CD-MOF particles were obtained by centrifugation, washing with isopropanol for several times to remove the residual reagents according to the published literatures[36,44], followed by drying under vacuum at room temperature for 24 h.

A series of ketoprofen-loaded CD-MOF (CD-MOF-K) particles were prepared by a co-crystallisation method, denoted as CD-MOF-K-A, CD-MOF-K-B and CD-MOF-K-C (Table 1). Briefly, ketoprofen was dissolved in methanol (20 mg/mL) and mixed with the solution of γ-CD and KOH. The other experimental procedures were similar to the preparation of CD-MOF.

In order to make a comparison, the commercial formulation (CF) was prepared. Raw ketoprofen was micronized using a jet mill (AO, Youte Powder Mechanical Equipment Co., Ltd., China) with the pressure of 0.4 MPa, and the feeding rate was about 100 mg/min. The micronized ketoprofen was manually mixed evenly with the commercial nonporous carrier (InhaLac® 230) at a ratio of 1:39 (*w*/*w*).

2.4. Characterization

2.4.1. Scanning electron microscopy (SEM)

The morphologies of different kinds of CD-MOF-K and CF were characterized by a scanning electron microscopy (SEM, JSM-6330F, JEOL, Japan). Before characterization, the samples were placed on a copper stub using double-sided adhesive tape and coated with a gold film under vacuum.

2.4.2. Powder X-ray diffraction (PXRD)

The crystallinity of the powders was evaluated using an X-ray diffractometer (D2 PHASER, Bruker, Germany) equipped with the PXRD V1.0 software. The samples were scanned from 5° to 30° (2θ) at 30 kV and 10 mA with Cu Kα radiation. The step size was 0.0142° (2θ) and the dwell time was 0.1 s.

2.4.3. Particle size analysis

The particle size of the samples was measured by a laser diffraction particle size analyzer (Malvern Mastersizer 2000, Malvern, UK). Prior to the measurement, the samples were dispersed by a compressed air stream with air pressure of 4.0 bar.

2.4.4. Nitrogen adsorption-desorption analysis

The nitrogen adsorption-desorption isotherms of the samples were recorded by a surface area and pore size analyzer (ASAP 2460, Micromeritics, USA). Before the measurement, the samples were dried under vacuum to remove the residual solvent at 50 °C for 24 h, and degassed under vacuum at 50 °C for 6 h. The surface area and pore size of the sample was calculated using Microactive for ASAP 2460 software according to the nitrogen adsorption-desorption isotherms.

2.5. In vitro drug release study

For *in vitro* drug release study, the simulated lung fluid (SLF) was used to simulate the physiological environment in lungs, which was composed of 0.02% DPPC, 0.02% potassium dihydrogen phosphate, 0.318% disodium hydrogen phosphate, 0.02% potassium chloride, 0.01% magnesium chloride, 0.01% calcium chloride, and 0.80% sodium chloride (all *w*/*v*)[45]. Samples containing 1 mg of ketoprofen and 1 mL of SLF were enclosed in the dialysis bags and incubated in 30 mL of SLF. After incubation in a constant temperature shaker (100 rpm, 37 °C), 1 mL of the release medium was withdrawn at predetermined time points, and then equivalent of fresh release medium was compensated for sample losing.

The obtained release medium was filtered through 0.22 μm membrane and analyzed by a high performance liquid chromatography system (HPLC, LC-20, Shimadzu, Japan). The mobile phase consisted of methanol and 0.02 mol/L monopotassium phosphate buffer solution (80:20, *v*/*v*) with a flow rate of 1 mL/min.

Table 1 Synthesis conditions of CD-MOF-K-A, CD-MOF-K-B and CD-MOF-K-C.

Sample	V_w:V_{km}:V_m	Water bath temperature (°C)	Water bath time (h)	Standing time (h)
CD-MOF-K-A	10:6:15	50.0	0.5	4.0
CD-MOF-K-B	10:6:6	50.0	0.5	2.0
CD-MOF-K-C	10:6:0	50.0	1.0	2.0

V_w is the volume of water, V_{km} is the volume of ketoprofen methanol solution, and V_m is the volume of methanol.

Twenty microliters of the release medium were injected into a C18 column (5 μm, 250 mm × 4.6 mm, Diamonsil, Beijing, China), and detected at 258 nm. The column temperature was set at 40 °C.

2.6. *In vitro aerodynamic performance analysis*

The aerodynamic performance of the samples was evaluated using the next generation pharmaceutical impactor (NGI, Copley Scientific, Nottingham, UK). The sample (10 mg) was loaded into a size 3 hydroxypropyl methyl cellulose capsule (Capsugel Ltd., Suzhou, China), which was placed into a Turbospin® device (PH & T, Milan, Italy). The inhaler device was connected to the NGI using a mouthpiece adaptor. Prior to measurement, the flow rate was set to 60 L/min and the actuation time was set to 4 s. Ten capsules were used for one measurement. After aerosolization, the inhaler device, mouthpiece, throat, pre-separator, and all stages were washed with deionized water separately. The amounts of ketoprofen in different parts of NGI were determined by HPLC. The aerodynamic parameters including fine particle fraction (FPF), mean mass aerodynamic diameter (MMAD), and geometric standard deviation (GSD) were analyzed by CITDAS software (version 3.00, Copley Scientific). In addition, the emitted dose was also evaluated by NGI with a flow rate of 60 L/min for 1 s, and the process was repeated four times.

2.7. *Finite element analysis*

Finite element analysis was performed to investigate the mechanism of different aerosolization performance between CD-MOF-K-A and CF. Briefly, the model of NGI was established according to its actual size in flow field by finite element method. The number of particles was set as 1500, and the diameters of all particles were set as 2 μm, which was in good agreement with the actual size of samples. The densities of CD-MOF-K-A and CF were set as 0.5 and 0.9 g/cm^3 according to their actual values, respectively. The motion of particles in NGI model followed Newton's second law in Eq. (1):

$$m\frac{\mathrm{d}^2x}{\mathrm{d}t^2} = F\left(t, x, \frac{\mathrm{d}x}{\mathrm{d}t}\right) \tag{1}$$

where x represents the position of particles, m is the mass of particles, and F represents all forces on particles in the flow field, which include the gravitational force and drag force. In addition, in order to simulate the impact of porous structure for CD-MOF-K-A on aerosolization performance, the lift force was applied to CD-MOF-K-A. The simulated deposition rates of particles in NGI model were recorded.

2.8. *Cytotoxicity assay*

The cytotoxicity of ketoprofen, CD-MOF, and CD-MOF-K was tested on A549 and Calu-3 cells using cell counting kit-8 (CCK-8, Dojindo, Japan). The A549 and Calu-3 cells were seeded in 96-well microplates at a density of 5×10^3 and 1×10^4 cells per well, respectively. After culturing at 37 °C for 24 h, the culture medium was replaced with 100 μL of fresh medium containing samples with different concentrations ranging from 10 to 500 μg/mL. The fresh medium without sample was employed as the control. After incubation for another 24 h, the old medium was removed, and 110 μL of fresh medium containing 10 μL of CCK-8 solution was added into each well and incubated. The ultraviolet adsorption value of the samples was measured at 450 nm with a plate reader (Epoch2, BioTek, Winooski, USA). The cell viability was calculated as the percentage of the treated cells to the untreated control cells.

2.9. *Hemolysis test*

The fresh blood was collected from an SD rat donor. The red blood cells were obtained by centrifugation of the blood at 1506×g for 10 min, and washed with phosphate buffered solution (PBS) for three times. Then, the particles were suspended in PBS at the concentrations ranging from 31.3 to 4000 μg/mL. The solution was mixed with equal volume of PBS containing the red blood cells (5%, *v*/*v*), and incubated at 37 °C for 1 h. After centrifugation at 1506×g for 10 min, 30 μL of supernatant was mixed with 100 μL of PBS, and measured at 570 nm using a plate reader (ELx800, BioTek). PBS and 2% Triton X-100 were employed as the negative group and positive group, respectively. The hemolysis ratio was calculated as Eq. (2):

$$\text{Hemolysis ratio}\ (\%) = \frac{\mathrm{OD_s} - \mathrm{OD_n}}{\mathrm{OD_p} - \mathrm{OD_n}} \times 100 \tag{2}$$

where $\mathrm{OD_s}$, $\mathrm{OD_n}$, and $\mathrm{OD_p}$ are the absorbance values of the sample, negative group, and positive group, respectively.

2.10. *Lung function evaluation*

The SD rats (180−220 g) were randomly divided into four groups with twelve rats per group, and anesthetized by intraperitoneal injection of 20% urethane solution (*v*/*v*, 5 mL/kg). Three groups were intratracheally administered with CD-MOF, CD-MOF-K, and CF (40 mg/kg). The sample was sprayed using a dry powder insufflator (DP-4R, Pen-Century Inc., Wyndmoor, USA). Another group without any treatment was regarded as control group. After administration, six rats were evaluated by using the lung function system (RC system, Buxco, Wilmington, USA) at 1 and 8 h, respectively. Briefly, the rat trachea was exposed and cut a small incision on it. Then, an endotracheal tube was inserted into the trachea and connected to a ventilator to maintain the respiration of rats. The rats were then placed in a whole body plethysmograph, and the relevant values were recorded by the lung function system.

2.11. *In vivo lung injury markers measurement*

The SD rats (180−220 g) were randomly divided into nine groups with six rats in each group: blank group (no drug treatment), positive control group (LPS-24 h group and LPS-48 h group), CD-MOF-24 h group, CD-MOF-48 h group, CD-MOF-K-24 h group, CD-MOF-K-48 h group, CF-24 h group, and CF-48 h group. After anesthetized by intraperitoneal injection with 20% urethane solution (*v*/*v*, 5 mL/kg), the rats were intratracheally administered with CD-MOF, CD-MOF-K, CF (40 mg/kg) by a dry powder insufflator (DP-4R, Penn-Century Inc.), or LPS solution (3 mg/kg) by an endotracheal aerosolization device (HRH-MAG4, HUIRONGHE, Beijing, China). At 24 and 48 h post administration, an endotracheal tube was inserted into the exposed rat trachea. Then, the lungs were infused with 1 mL of PBS *via* a tube, and bronchoalveolar lavage was carried out for three times. The bronchoalveolar lavage fluid (BALF) was centrifuged at 7870×g for 10 min, and the supernatant was collected and stored at −80 °C for further analysis.

The levels of the inflammatory cytokines (IL-1β, IL-6, MIP-1α and TNF-α) in BALF were determined by a specialized assay kit

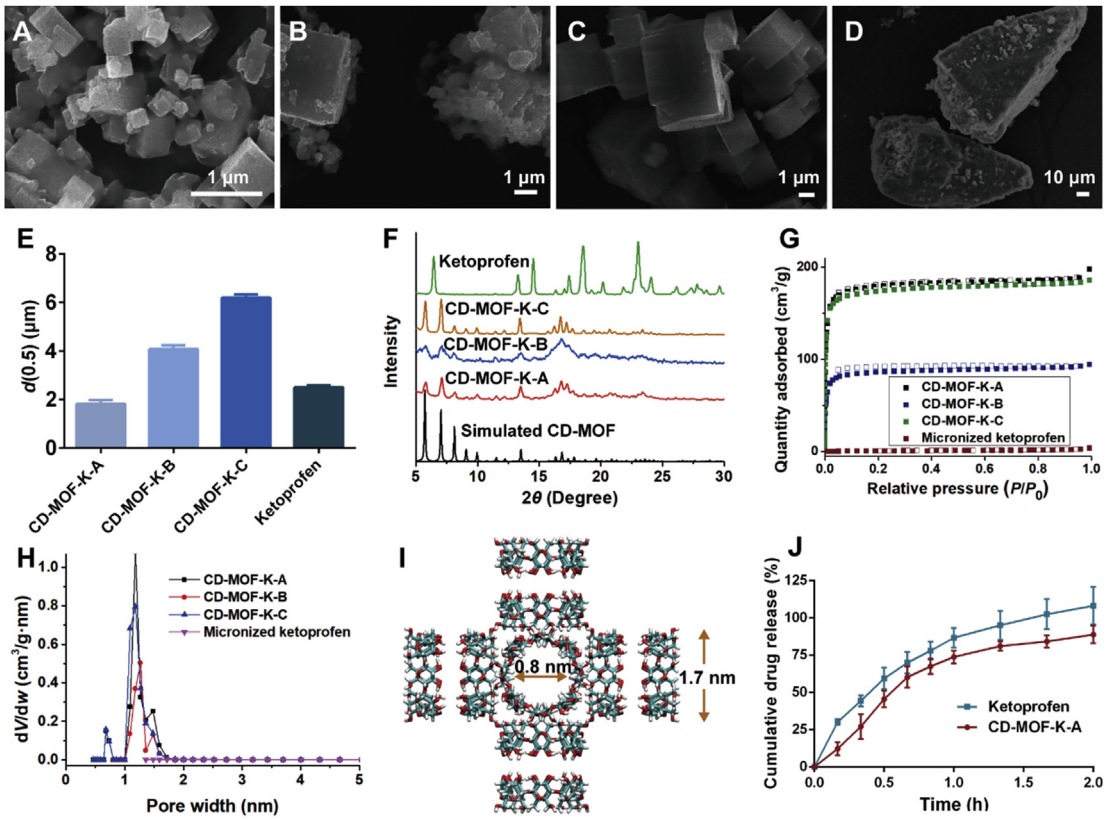

Figure 1 SEM images of (A) CD-MOF-K-A, (B) CD-MOF-K-B, (C) CD-MOF-K-C, and (D) CF. (E) The median diameters of CD-MOF-K-A, CD-MOF-K-B, CD-MOF-K-C, and micronized ketoprofen (data are expressed as mean ± SD, $n = 3$). (F) PXRD patterns of simulated CD-MOF, CD-MOF-K-A, CD-MOF-K-B, CD-MOF-K-C, and ketoprofen. (G) N_2 adsorption-desorption isotherms and (H) pore size distributions of CD-MOF-K-A, CD-MOF-K-B, CD-MOF-K-C, and micronized ketoprofen. (I) The schematic illustration of the structure of CD-MOF. (J) The drug release profiles for CD-MOF-K-A and ketoprofen at 37 °C. The release medium was simulated lung fluid (data are expressed as mean ± SD, $n = 3$).

(RECYTOMAG-65K, Merck Millipore, Billerica, USA) according to the protocols. Lactate dehydrogenase (LDH) was quantified by a LDH assay kit (BC0685, Solarbio, Beijing, China), and total protein was quantified by a BCA protein quantification kit (20201ES76, YESEN, Shanghai, China).

2.12. *Histological analysis*

As described in Section 2.10, CD-MOF, CD-MOF-K, CF, and LPS solution were administrated to rats through lungs. The rats were sacrificed at different time points (24 and 48 h) after administration. Then, the major organs (lung, heart, liver, spleen, and kidney) were harvested and fixed with 10% formalin. The fixed organs were embedded in paraffin and sliced for hematoxylin−eosin (HE) staining. The stained organs were observed by a digital scanner (Pannoramic 250, 3DHISTECH, Budapest, Hungary).

2.13. *Ex vivo fluorescence imaging*

In order to further investigate the biodistributions after administration. Ketoprofen was replaced with fluorescent probe rhodamine B to prepare samples, denoted as CD-MOF-R-A and CD-MOF-R-C. The SD rats (180−220 g) were randomly divided into three groups, and anesthetized by intraperitoneal injection of 20% urethane solution (*v*/*v*, 5 mL/kg). Three groups were intratracheally administered with CD-MOF-R-A, CD-MOF-R-C, and CF (40 mg/kg), respectively. The rats were sacrificed at different time points (0.5, 1, 2, 4, and 8 h) after administration. The major organs (lung, heart, liver, spleen, and kidney) were excised and imaged using a fluorescent imaging system (NightOWL II LB983, Berthold, Bad Wildbad, Germany). The excitation wavelength was set as 475 nm and the emission wavelength was set as 600 nm.

2.14. *Statistical analysis*

Data were expressed as mean ± standard deviation (SD). The statistical comparison was performed using one-way analysis of variance (ANOVA) test by Graphpad Prism 6.02 (Graphpad Software, San Diego, CA, USA). P values < 0.05 were considered statistically significant.

3. Results and discussion

3.1. *Synthesis and characterization of CD-MOF-K*

The particle size of CD-MOF was delicately tailored by optimizing the reaction parameters during the synthesis process including volume ratio of methanol to water, concentration of CTAB, water bath time, and the standing time (Supporting

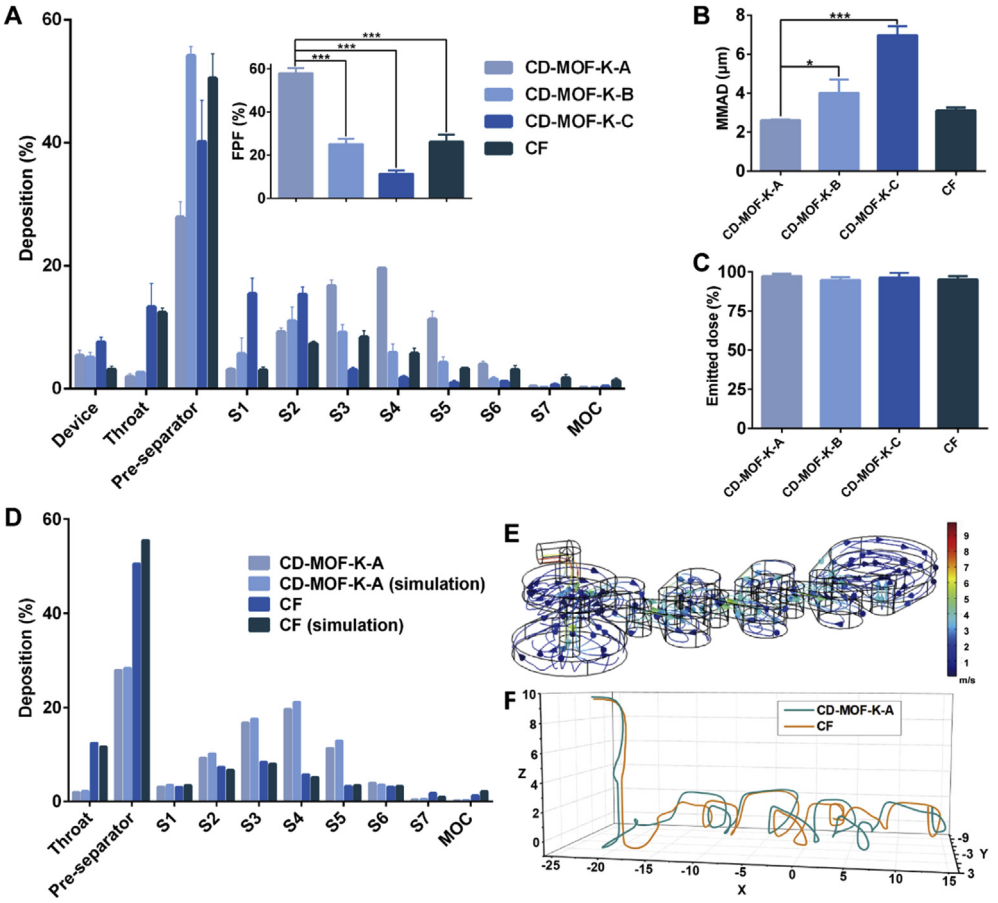

Figure 2 (A) *In vitro* pulmonary deposition patterns of CD-MOF-K-A, CD-MOF-K-B, CD-MOF-K-C, and CF. Inset shows the FPF values of different samples (data are expressed as mean ± SD, $n = 3$). (B) Mass median aerodynamic diameters of CD-MOF-K-A, CD-MOF-K-B, CD-MOF-K-C, and CF (data are expressed as mean ± SD, $n = 3$). (C) Emitted dose of CD-MOF-K-A, CD-MOF-K-B, CD-MOF-K-C, and CF (data are expressed as mean ± SD, $n = 10$). (D) The experimental and simulated deposition rates of CD-MOF-K-A and CF in different stages of NGI. The simulation was performed using finite element method. (E) The velocity field of the NGI model by finite element method. (F) The trajectories of CD-MOF-K-A and CF particles in NGI model. Significant difference is regarded as $P < 0.05$, $^{*}P \leq 0.05$, $^{**}P \leq 0.01$, $^{***}P \leq 0.001$.

Information Figs. S1−S4). The results showed that the volume ratio of methanol to water was the most important factor affecting the particle size. As shown in Fig. S1, the median particle diameter decreased significantly when the volume ratio of methanol to water increased from 1:10 to 6:10. During the synthesis of CD-MOF, the added methanol in the solution led to the supersaturation of precursors, subsequently enabling the formation of the small nuclei which could act as centers for further crystal growth. A high ratio of methanol to water increased the supersaturation level, and induced the generation of a large number of nuclei *via* burst nucleation, which ultimately resulted in smaller particles[36,46]. Furthermore, the particle size of CD-MOF was also reduced with the increasing concentration of CTAB (Fig. S2), because CTAB could cover the surface of the existing small particles to inhibit the crystal growth due to the steric hindrance effect. Meanwhile, the water bath time and standing time did not show significant influence on the particle size of CD-MOF (Figs. S3 and S4).

According to the results above, a series of CD-MOF-K particles with different size distribution were synthesized *in situ via* a one-step co-crystallisation method and denoted as CD-MOF-K-A, CD-MOF-K-B and CD-MOF-K-C. During this process, some interactions might participate and promote drug loading into the cavity of CD-MOF, including the hydrogen bonds between the carboxyl groups of ketoprofen and hydroxyl groups of γ-CD and the strong electrostatic interactions between ketoprofen and potassium ions[36,37]. The drug loading contents of CD-MOF-K-A, CD-MOF-K-B, and CD-MOF-K-C were 2.77%, 2.89%, and 2.17%, respectively (Supporting Information Fig. S5). In order to make a comparative study, ketoprofen was micronized *via* a jet mill and then mixed with the commercial dry powder inhaler carrier (InhaLac® 230, Wasserburg, Germany), named CF. The median diameter of the commercial carrier was between 70 and 110 μm, and its Carr's index was 18% according to the product information. During the inhalation process, the micronized ketoprofen particles would detach from the carrier and reach the deep lungs, while the carrier would impact in the throat and be swallowed with no access to lungs[47]. Therefore, the properties of micronized ketoprofen are important for the aerodynamic behavior of CF, which were systematically characterized.

The morphologies of CD-MOF-K and CF were observed by SEM (Fig. 1A–D). The results showed that CD-MOF-K with different particle size were cubic in appearance. Their median diameters were 1.82, 4.07 and 6.20 μm, respectively (Fig. 1E),

which demonstrated that the particle size of CD-MOF could be adjusted by changing synthetic conditions. The S_{pan} value of CD-MOF-K-B was larger than those of CD-MOF-K-A and CD-MOF-K-C, indicating that the particle size of CD-MOF-K-B was inhomogeneous (Supporting Information Table S1). Moreover, Fig. 1B showed that CD-MOF-B particles were easy to agglomerate. The SEM image of CF (Fig. 1D) showed that the micronized ketoprofen was successfully adsorbed on the surface of the commercial carriers. The median diameter of micronized ketoprofen was 2.50 μm, which was similar to that of CD-MOF-K-A.

The crystalline state of CD-MOF-K and ketoprofen was investigated by PXRD. As shown in Fig. 1F, the evident peaks of all CD-MOF-K were at 5.8°, 7.1°, 8.2°, 13.5° and 16.8°, which were in good agreement with the data reported in the literature[36,44]. Moreover, no crystalline characteristic peaks of ketoprofen were observed in the PXRD patterns of CD-MOF-K, indicating that ketoprofen might be loaded into CD-MOF in molecular state because of the spatial confinement of the pores of CD-MOF.

The surface area of the samples was evaluated by the nitrogen adsorption-desorption analysis (Fig. 1G). The Brunauer–Emmett–Teller (BET) surface area of CD-MOF-K-A, CD-MOF-K-B, and CD-MOF-K-C were 732, 350, and 703 m^2/g, respectively, which was much higher than that of micronized ketoprofen, indicating the porosity of CD-MOF-K. The pore width of CD-MOF-K was approximately 1.3 nm with homogeneous distribution (Fig. 1H), which was consistent with the structure of CD-MOF (Fig. 1I).

Moisture sorption profiles of samples were shown in Supporting Information Fig. S6. No obvious difference was found in the moisture sorption profiles among CD-MOF-K-A, CD-MOF-K-B, and CD-MOF-K-C. The absorbed water of CD-MOF-K particles increased with the increasing relative humidity, and the water absorptions were higher than 18% at 95% relative humidity for all groups. Therefore, it is recommended to store CD-MOF-K powders in low humidity environment.

The *in vitro* drug release profiles of CD-MOF-K-A and ketoprofen were investigated in SLF to simulate the lung conditions. As depicted in Fig. 1J, there was no significant difference between the drug release profiles of CD-MOF-K-A and ketoprofen. Ketoprofen showed approximately 100% drug release within 2 h, and the amount of ketoprofen released from CD-MOF-K-A within 2 h was 89%. The fast release rate of ketoprofen can be explained by the following two reasons. Firstly, ketoprofen is a weakly acidic drug with pH-dependent solubility[48] and the buffer salts in SIF can effectively improve its dissolution rate. Secondly, DPPC in SIF is the main component of lung surfactant[49], which also significantly increased the solubility of ketoprofen.

3.2. *In vitro aerodynamic performance*

NGI was used for the *in vitro* assessment of drug delivery efficiency of inhalation particles. Generally, the particles with different aerodynamic diameter could be deposited in different collection cups, which showed a strong correlation with the regional deposition in lungs[50]. The deposition patterns of samples at different cups of NGI were shown in Fig. 2A. The deposition rate of CD-MOF-K-A at stages 3–6 was much higher than that of CD-MOF-K-B and CD-MOF-K-C, while the drug deposition rate at pre-separator for CD-MOF-K-B was higher than those for CD-MOF-K-A and CD-MOF-K-C, which was likely due to the particle agglomeration of CD-MOF-K-B. The aerosolization efficiency was further characterized by FPF and MMAD (Fig. 2B), which were calculated by the CITDAS software. FPF represents the mass percentage of the emitted particles which are predicted to be delivered to the lungs. MMAD is defined as the aerodynamic diameter of the median aerosol particles. The FPF value of CD-MOF-K-A was 57.99%, which was significantly higher than that of CD-MOF-K-B (25.14%) and CD-MOF-K-C (11.38%). It was found that the FPF values of CD-MOF-K increased with the decreasing median diameters, which suggested that the aerodynamic performance of CD-MOF-K

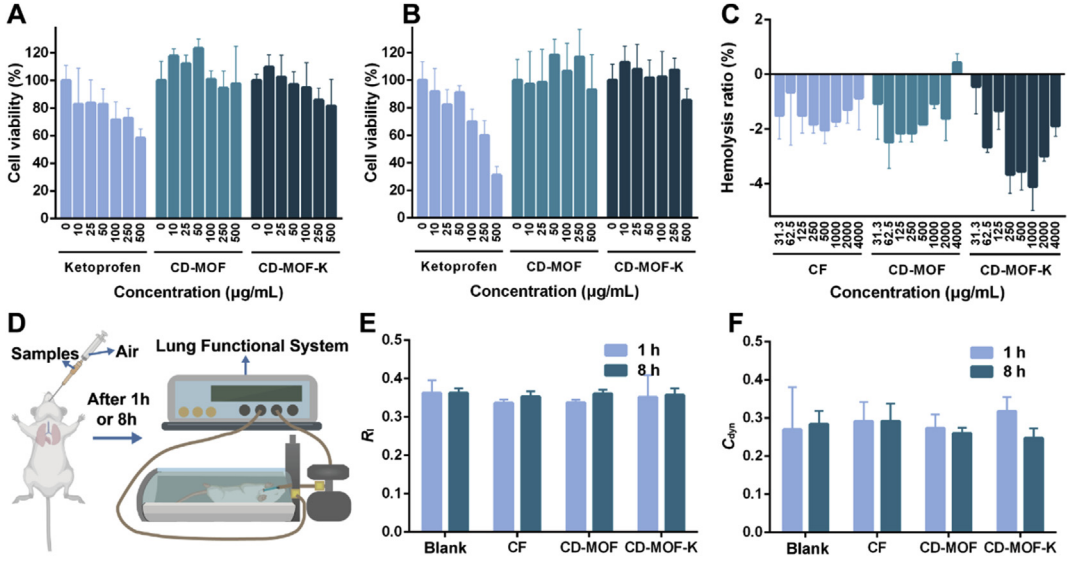

Figure 3 Cell viabilities of (A) A549 cells and (B) Calu-3 cells after incubated with various concentrations of ketoprofen, CD-MOF, CD-MOF-K for 24 h (data are expressed as mean ± SD, $n = 6$). (C) Hemolysis ratios of CF, CD-MOF, CD-MOF-K at various concentrations (data are expressed as mean ± SD, $n = 3$). (D) Illustration of intratracheally administration of samples to rats and the evaluation of lung function of rats. The (E) R_l and (F) C_{dyn} values of rats after pulmonary delivery of different samples for 1 and 8 h (data are expressed as mean ± SD, $n = 6$).

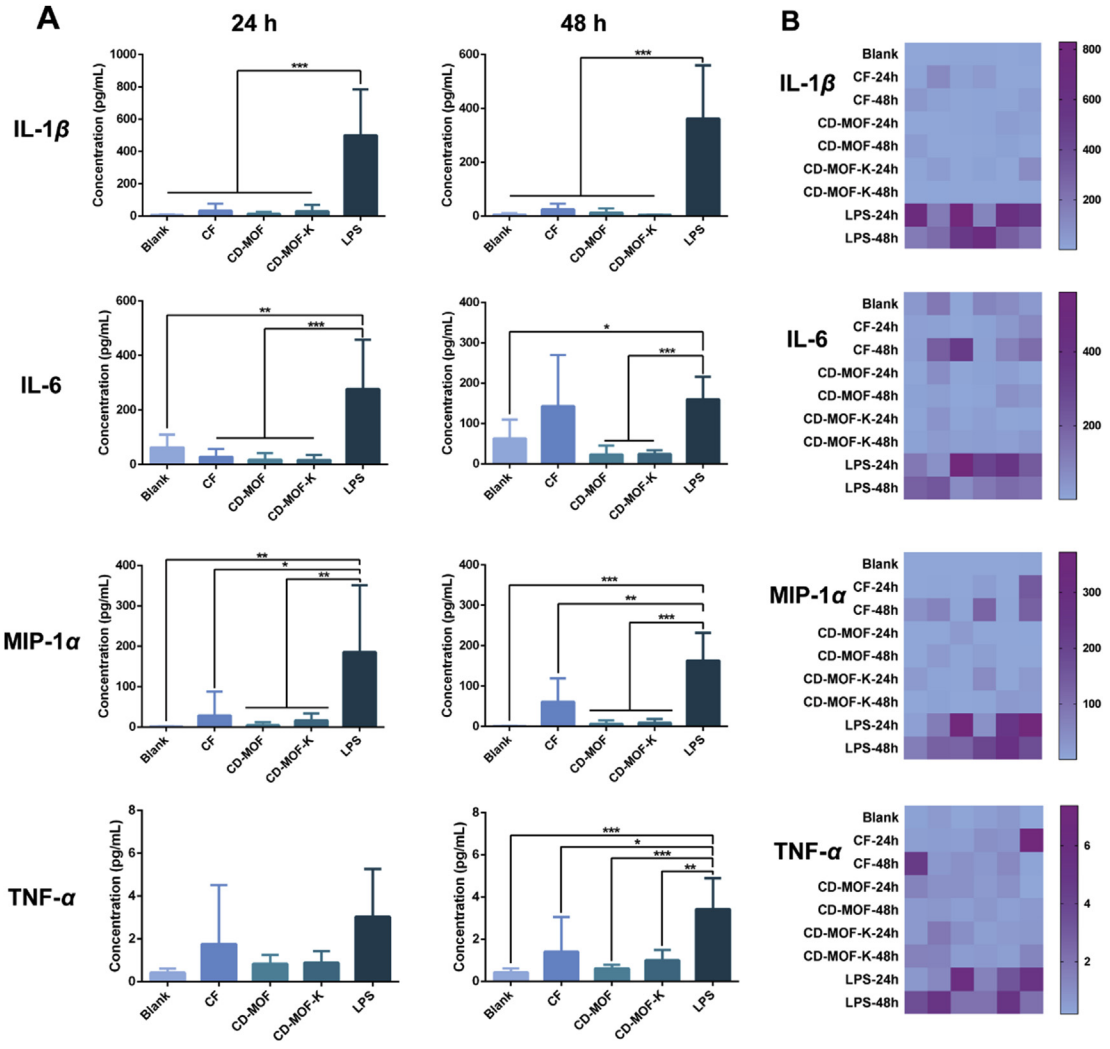

Figure 4 (A) Concentrations of various inflammatory cytokines in BALF of rats after pulmonary delivery of different samples for 24 and 48 h (data are expressed as mean ± SD, $n = 6$). Significant difference is regarded as $P < 0.05$, $*P \leq 0.05$, $*P \leq 0.01$, $***P \leq 0.001$. No significant difference was found among blank, CF, CD-MOF and CD-MOF-K groups. (B) Heatmaps of various inflammatory cytokines in BALF of different groups.

could be improved by particle size engineering *via* different synthesis conditions. Moreover, the MMAD of CD-MOF-K-A (1.82 μm) was much lower than that of CD-MOF-K-B (4.07 μm) and CD-MOF-K-C (6.20 μm), which were consistent with their median diameters determined by the laser diffraction particle size analyzer. Compared with the CD-MOF in the previous study[51], CD-MOF-K-A showed a higher FPF value, which might be attributed to the smaller median diameter.

The aerodynamic performance of CF was also evaluated as a comparison. The results showed that the FPF value of CD-MOF-K-A was 2.21-fold higher than that of CF, though the median diameter of CD-MOF-K-A was similar to that of micronized ketoprofen, indicating that CD-MOF had a superior aerodynamic behavior as compared with the commercial dry powder inhaler carrier. The difference in aerodynamic behaviors between CD-MOF-K-A and CF can be explained by the following reasons. Firstly, the homogeneous nanoporous structure of CD-MOF could greatly improve the aerodynamic performance. On one hand, the nanoporous structure remarkably reduced the density of particles (Supporting Information Table S2). On the other hand, the porous particles tended to aggregate less and disaggregate more easily under shear forces than non-porous particles[52], which was attributed to the reduced contact area and interparticulate interactions, ultimately resulting in excellent aerodynamic performance. Moreover, the unique cubic morphology of CD-MOF-K might be favorable to lower the interparticulate interactions and facilitated better particle dispersion.

The emitted dose of each formulation was also measured by NGI, all of which were higher than 90% (Fig. 2C). Because of its excellent aerodynamic behavior, CD-MOF-K-A was chosen as the optimized formulation and used for further investigation.

In order to investigate the specific motion of CD-MOF-K-A and CF in NGI, the NGI model was established in flow field by finite element method according to its actual size (Supporting Information Fig. S7). As shown in Fig. 2D, the simulated deposition rates in NGI were in good agreement with the experiment data, indicated the successful simulation. The velocities of particles in various positions of NGI model were different (Fig. 2E), and the velocities were high when air entered into the next stage from one stage through the holes. The trajectories of CD-MOF-K-A and CF particles in NGI model were tracked (Fig. 2F), which

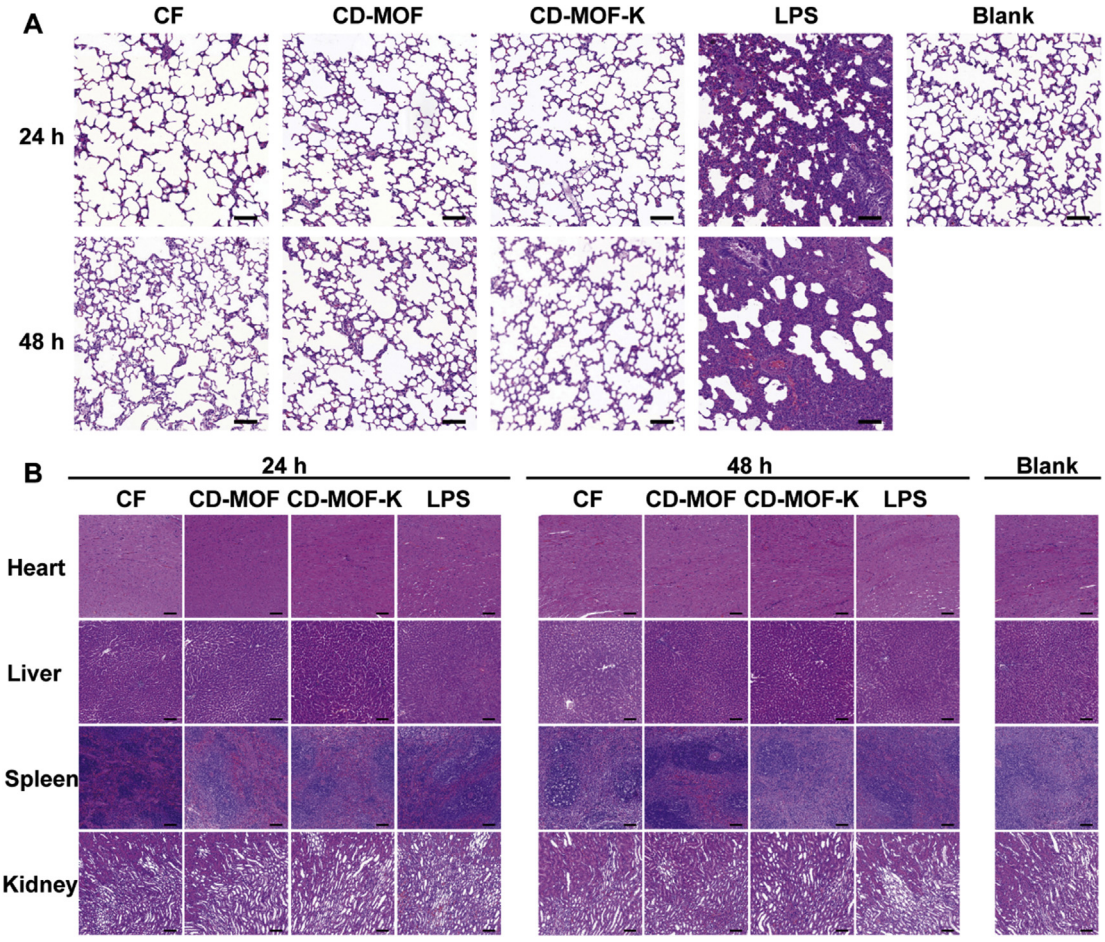

Figure 5 (A) Histological images of lungs excised after pulmonary delivery of different samples into rats at different time points (scale bar: 100 μm for all panels). (B) Histological images of organs (heart, liver, spleen, and kidney) excised after pulmonary delivery of different samples into rats at different time points (scale bar: 100 μm for all panels).

showed that the trajectory of CD-MOF-K-A was generally higher than that of CF, and the drag and lift force of CD-MOF-K-A was larger than that of CF (Supporting Information Fig. S8). The higher trajectory confirmed the better aerosolization performance of CD-MOF-K-A particles, which was attributed to their homogenous nanoscale pores.

3.3. The cytocompatibility and lung function evaluation

Although a large number of pulmonary drug delivery carriers have been investigated, the current list of excipients approved by FDA for pulmonary drug delivery is very limited. Good biocompatibility is a prerequisite for the application of pulmonary drug delivery carriers. As a new type of potential pulmonary drug delivery carrier, the toxicity of CD-MOF should be stringently evaluated.

The cytocompatibility of pure ketoprofen, CD-MOF, and CD-MOF-K was evaluated on A549 and Calu-3 cells, respectively (Fig. 3A and B). As shown in Fig. 3A, the viability of A549 cells presented a gradual decrement trend with the increasing concentration of ketoprofen. The cell viability value was 58.32% at a ketoprofen concentration of 500 μg/mL. In contrast, CD-MOF did not cause significant inhibition of cell growth. The cell viability values were approximately 100% at all ranges of concentration, indicating its excellent cytocompatibility. Moreover, the cell viability values were higher than 100% at low concentrations for CD-MOF (10−50 μg/mL). CD-MOF is mainly composed of γ-cyclodextrin, a kind of nature cyclic oligosaccharide, which may promote the proliferation of cells as nutrient at low concentrations. CD-MOF-K did not show obvious cytotoxic effect towards A549 cells, and the cell viability values were all higher than 80% at the concentrations ranging from 0 to 500 μg/mL. The slight inhibition of cell growth was attributed to ketoprofen loaded into CD-MOF.

The viability of Calu-3 cells incubated with ketoprofen, CD-MOF, and CD-MOF-K was further evaluated (Fig. 3B). The cytotoxic effects of samples towards Calu-3 cells were similar to those towards A549 cells, which further demonstrated the great cytocompatibility of CD-MOF.

For pulmonary administration, drugs will enter the blood circulation through the capillary network of lung. Therefore, it is necessary to investigate the blood compatibility of CD-MOF. The hemolysis ratio of positive group (2% Triton X-100) was set as 100%. All the experimental groups of red blood cells did not show hemolytic phenomenon after incubated with samples at concentrations ranging from 31.3 to 4000 μg/mL, with the hemolysis ratios less than 0.5% (Fig. 3C). The negative values of hemolysis ratio were probably caused by the errors from experimental

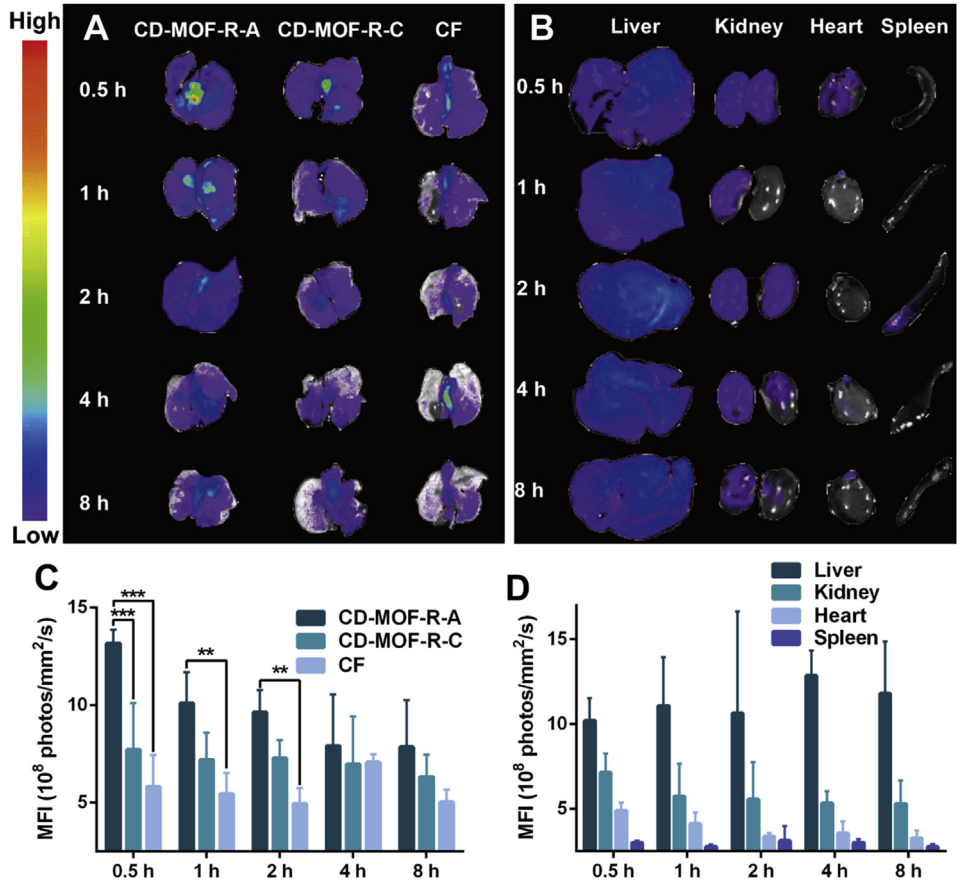

Figure 6 (A) The fluorescence images of lungs at different time points after pulmonary delivery of different samples into rats. (B) The fluorescence images of the major organs (liver, kidney, heart, and spleen) at different time points after pulmonary delivery of CD-MOF-R-A into rats. (C) MFI values of lungs at different time points after pulmonary delivery of different samples into rats (data are expressed as mean ± SD, $n = 3$). Significant difference is regarded as $P < 0.05$, $^*P \leq 0.05$, $^{**}P \leq 0.01$, $^{***}P \leq 0.001$. (D) MFI values of the major organs (liver, kidney, heart, and spleen) at different time points after pulmonary delivery of CD-MOF-R-A into rats (data are expressed as mean ± SD, $n = 3$).

process itself, which was also reported in other literature[53]. These results demonstrated the good blood compatibility of CD-MOF.

In order to assess the airway and lung responsiveness of the samples, the lung function of rats intratracheally administered by different samples was evaluated by lung function system (Fig. 3E and F). If the airway and lung responsiveness of the pulmonary drug delivery carrier is high, the inhalation and exhalation may be obstructed by swelling in airway membranes and excessive mucus production, leading to cough, asthma and adverse reactions. Lung resistance (R_l) and dynamic lung compliance (C_{dyn}) are two important parameters regarding lung function. The large R_l value indicates the alterations in the lung periphery and narrowing of the conducting airways, and the small C_{dyn} value reflects lung unit derecruitment caused by the airway closure[54]. Compared with the blank group, both the values of R_l and C_{dyn} for CD-MOF group, CD-MOF-K group, and CF group did not show any statistical differences at 1 and 8 h. This demonstrated that the airway and lung responsiveness of CD-MOF carrier were low, and CD-MOF did not significantly affect the lung function of rats after pulmonary administration in a short period.

3.4. *In vivo inhalation toxicity and inflammatory effects*

In order to investigate the inhalation toxicity and the inflammatory effects of CD-MOF, the concentrations of inflammatory cytokines (IL-1β, IL-6, MIP-1α, and TNF-α) in BALF were measured (Fig. 4). If the sample is irritating to respiratory tract and lung, it will stimulate inflammatory response of the body and the expression of inflammatory cytokines will be upregulated. LPS was administrated as the positive control, which could induce the obvious inflammatory effects[55]. The blank group without treatment was the negative control for these measurements.

The concentrations of inflammatory cytokines in BALF of rats administrated with different samples after 24 h were shown in Fig. 4A. The concentrations of IL-1β, IL-6, MIP-1α, and TNF-α for LPS group were much higher than those of blank group, CF group, CD-MOF group, and CD-MOF-K group, indicating that the inflammatory effects were successfully induced by LPS. There was no statistical difference on the levels of inflammatory cytokines among blank group, CF group, CD-MOF group, and CD-MOF-K group. These results indicated that CD-MOF and commercial carrier would not induce severe inflammatory effects. The levels of inflammatory cytokines in BALF after 48 h were further evaluated. The levels of IL-1β, IL-6, MIP-1α, and TNF-α for LPS group were much higher than those for other groups. It should be noted that the concentrations of inflammatory cytokines at 48 h for CF group were slight higher than those for blank group, CD-MOF group, and CD-MOF-K group, indicating that the commercial carrier might cause mild irritation.

The protein concentrations and LDH activity in BALF at 48 h were also evaluated (Supporting Information Figs. S9 and S10). The protein concentrations and LDH activity of LPS group were higher than those of other groups, which were consistent with the results of inflammatory cytokines, demonstrating the excellent biocompatibility of CD-MOF.

The histological analysis of the lungs treated with different samples was evaluated (Fig. 5A). Compared with blank group, the alveolar structure of LPS group significantly changed. Most of the alveolar luminal space was obliterated with the thickening of alveolar septum. Severe pulmonary congestion and inflammation response could be observed in the histological image of LPS group. By contrast, no obvious inflammation reactions and histological abnormalities were observed in blank group, CD-MOF group, and CD-MOF-K group, which were consistent with the results of inflammatory cytokines. Histological images of the sections of major organs (heart, liver, spleen, and kidney) were also observed (Fig. 5B). No noticeable signals of organ damage were observed for all groups, suggesting that CD-MOF at the test doses would not cause apparent histological abnormalities or lesions. These results demonstrated the good biocompatibility of CD-MOF as a pulmonary drug delivery carrier.

3.5. *Ex vivo fluorescence imaging*

In order to investigate the *in vivo* fate of drug delivery system after pulmonary administration, rhodamine B was used as the fluorescence probe and loaded into the carriers by the similar preparation method with CD-MOF-K, denoted as CD-MOF-R-A and CD-MOF-R-C. As shown in Fig. 6A, the fluorescence intensities of lungs decreased over time in all groups. The mean fluorescence intensity (MFI) values of rhodamine B in lungs for CD-MOF-R-A were much higher than those for CD-MOF-R-C and CF (Fig. 6C), indicating that the deposition rate of CD-MOF-R-A in lungs was higher, which was consistent with the results of *in vitro* aerodynamic performance. These results indicated that the particle size of CD-MOF could be delicately tailored to achieve excellent aerodynamic performance, and the homogenous nanoporous structure of CD-MOF could efficiently improve the deposition rate of particles in lungs. The fluorescence intensities of other major organs for CD-MOF-R-A at various time points were investigated (Fig. 6B and D). The MFI values in livers and kidneys were higher than those in hearts and spleens, indicating that the fluorescence molecules encapsulated in CD-MOF would be metabolized and excreted *via* liver and kidney. Furthermore, the obvious fluorescence intensities of livers and kidneys appeared at 0.5 h suggested that the fluorescence molecules in CD-MOF-R-A would entered into the blood stream from lungs in a short time, followed by metabolism and excretion by liver and kidney.

4. Conclusions

In this study, nanoporous CD-MOF with different particle size was engineered and prepared delicately for pulmonary drug delivery. CD-MOF exhibited much better aerosolization performance compared with commercial nonporous carriers, which could be attributed to the decreased density of particles and weakened interparticulate interactions based on their homogenous nanoscale pores. The high lung deposition efficiency of CD-MOF was also confirmed in rats. Moreover, CD-MOF showed excellent biocompatibility, which would not affect the lung function and cause inflammatory reaction. Therefore, CD-MOF is a promising carrier for pulmonary drug delivery and has a broad application prospect in the treatment of respiratory diseases and lung cancer.

Acknowledgments

This work was supported by the National Natural Science Foundation of China (Grant No. 81803466), the Research and Development Plan for Key Areas in Guangdong Province (Grant No. 2019B020204002, China), the National Science and Technology Major Program (Grant No. 2017zx09101001, China), and Natural Science Foundation of Guangdong Province (Grant No. 2018A030310095, China). We gratefully acknowledged the assistance of Vikramjeet Singh in synthesis of CD-MOF.

Author contributions

Yixian Zhou designed and carried out the research, performed data analysis and wrote the manuscript. Boyi Niu carried out the research, performed data analysis and wrote the manuscript. Biyuan Wu, Sulan Luo, Jintao Fu, Yiting Zhao participated part of the experiments. Guilan Quan revised the manuscript. Xin Pan and Chuanbin Wu supervised the project. All of the authors have read and approved the final manuscript.

Conflicts of interest

The authors have no conflicts of interest to declare.

Appendix A. Supporting information

Supporting data to this article can be found online at https://doi.org/10.1016/j.apsb.2020.07.018.

References

1. Abdelaziz HM, Gaber M, Abd-Elwakil MM, Mabrouk MT, Elgohary MM, Kamel NM, et al. Inhalable particulate drug delivery systems for lung cancer therapy: nanoparticles, microparticles, nanocomposites and nanoaggregates. *J Control Release* 2018;**269**:374–92.
2. Ni R, Zhao J, Liu QY, Liang ZL, Muenster U, Mao SR. Nanocrystals embedded in chitosan-based respirable swellable microparticles as dry powder for sustained pulmonary drug delivery. *Eur J Pharmaceut Sci* 2017;**99**:137–46.
3. Patton JS, Fishburn CS, Weers JG. The lungs as a portal of entry for systemic drug delivery. *Proc Am Thorac Soc* 2004;**1**:338–44.
4. Lu DM, Hickey AJ. Pulmonary vaccine delivery. *Expert Rev Vaccines* 2007;**6**:213–26.
5. Karashima M, Sano N, Yamamoto S, Arai Y, Yamamoto K, Amano N, et al. Enhanced pulmonary absorption of poorly soluble itraconazole by micronized cocrystal dry powder formulations. *Eur J Pharm Biopharm* 2017;**115**:65–72.
6. Chen L, Okuda T, Lu XY, Chan HK. Amorphous powders for inhalation drug delivery. *Adv Drug Deliv Rev* 2016;**100**:102–15.
7. Pilcer G, Amighi K. Formulation strategy and use of excipients in pulmonary drug delivery. *Int J Pharm* 2010;**392**:1–19.
8. Chandel A, Goyal AK, Ghosh G, Rath G. Recent advances in aerosolised drug delivery. *Biomed Pharmacother* 2019;**112**:108601.
9. Hang ZL, Ni R, Zhou JY, Mao SR. Recent advances in controlled pulmonary drug delivery. *Drug Discov Today* 2015;**20**:380–9.

10. Yang Y, Bajaj N, Xu P, Ohn K, Tsifansky MD, Yeo Y. Development of highly porous large PLGA microparticles for pulmonary drug delivery. *Biomaterials* 2009;**30**:1947−53.
11. Li JQ, Zheng HL, Qin L, Xu EY, Yang LL, Zhang L, et al. *In vitro*−*in vivo* correlation of inhalable budesonide-loaded large porous particles for sustained treatment regimen of asthma. *Acta Biomater* 2019;**96**:505−16.
12. Kadota K, Yanagawa Y, Tachikawa T, Deki Y, Uchiyama H, Shirakawa Y, et al. Development of porous particles using dextran as an excipient for enhanced deep lung delivery of rifampicin. *Int J Pharm* 2019;**555**:280−90.
13. Lin XF, Kankala RK, Tang N, Xu PY, Hao LZ, Yang DY, et al. Supercritical fluid-assisted porous microspheres for efficient delivery of insulin and inhalation therapy of diabetes. *Adv Healthc Mater* 2019;**8**:1800910.
14. Chvatal A, Ambrus R, Party P, Katona G, Jójárt-Laczkovich O, Szabó-Révész P, et al. Formulation and comparison of spray dried non-porous and large porous particles containing meloxicam for pulmonary drug delivery. *Int J Pharm* 2019;**559**:68−75.
15. Kim HK, Chung HJ, Park TG. Biodegradable polymeric microspheres with "open/closed" pores for sustained release of human growth hormone. *J Control Release* 2006;**112**:167−74.
16. Hou AL, Li L, Huang Y, Singh V, Zhu CE, Pan X, et al. Fragmented particles containing octreotide acetate prepared by spray drying technique for dry powder inhalation. *Drug Deliv Transl Res* 2018;**8**:693−701.
17. Cai YP, Chen YH, Hong XY, Liu ZG, Yuan WE. Porous microsphere and its applications. *Int J Nanomed* 2013;**8**:1111−20.
18. Li X, Xue M, Raabe OG, Aaron HL, Eisen EA, Evans JE, et al. Aerosol droplet delivery of mesoporous silica nanoparticles: a strategy for respiratory-based therapeutics. *Nanomedicine* 2015;**11**:1377−85.
19. Hozayen WG, Mahmoud AM, Desouky EM, El-Nahass ES, Soliman HA, Farghali AA. Cardiac and pulmonary toxicity of mesoporous silica nanoparticles is associated with excessive ROS production and redox imbalance in Wistar rats. *Biomed Pharmacother* 2019;**109**:2527−38.
20. Furukawa H, Cordova KE, O'Keeffe M, Yaghi OM. The chemistry and applications of metal-organic frameworks. *Science* 2013;**341**:1230444.
21. Wang H, Lustig WP, Li J. Sensing and capture of toxic and hazardous gases and vapors by metal-organic frameworks. *Chem Soc Rev* 2018;**47**:4729−56.
22. Tian T, Zeng ZX, Vulpe D, Casco ME, Divitini G, Midgley PA, et al. A sol-gel monolithic metal-organic framework with enhanced methane uptake. *Nat Mater* 2018;**17**:174−9.
23. Jia HX, Yao YC, Zhao JT, Gao YY, Luo ZL, Du PW. A novel two-dimensional nickel phthalocyanine-based metal-organic framework for highly efficient water oxidation catalysis. *J Mater Chem A* 2018;**6**:1188−95.
24. Rui K, Zhao GQ, Chen YP, Lin Y, Zhou Q, Chen JY, et al. Hybrid 2D dual-metal-organic frameworks for enhanced water oxidation catalysis. *Adv Funct Mater* 2018;**28**:1801554.
25. Guan BY, Yu XY, Wu HB, Lou XW. Complex nanostructures from materials based on metal-organic frameworks for electrochemical energy storage and conversion. *Adv Mater* 2017;**29**:1703614.
26. Denny MS, Moreton JC, Benz L, Cohen SM. Metal-organic frameworks for membrane-based separations. *Nat Rev Mater* 2016;**1**:16078.
27. Desai AV, Manna B, Karmakar A, Sahu A, Ghosh SK. A water-stable cationic metal-organic framework as a dual adsorbent of oxoanion pollutants. *Angew Chem Int Ed* 2016;**55**:7811−5.
28. Duan CX, Li FE, Luo SJ, Xiao J, Li LB, Xi HX. Facile synthesis of hierarchical porous metal-organic frameworks with enhanced catalytic activity. *Chem Eng J* 2018;**334**:1477−83.
29. Chen W, Wu CS. Synthesis, functionalization, and applications of metal-organic frameworks in biomedicine. *Dalton Trans* 2018;**47**:2114−33.
30. Lan GX, Ni KY, Xu ZW, Veroneau SS, Song Y, Lin WB. Nanoscale metal-organic framework overcomes hypoxia for photodynamic therapy primed cancer immunotherapy. *J Am Chem Soc* 2018;**140**:5670−3.
31. Xiao JS, Chen SY, Yi J, Zhang HF, Ameer GA. A cooperative copper metal-organic framework-hydrogel system improves wound healing in diabetes. *Adv Funct Mater* 2017;**27**:1604872.
32. Kim SN, Park CG, Huh BK, Lee SH, Min CH, Lee YY, et al. Metal-organic frameworks, NH_2-MIL-88(Fe), as carriers for ophthalmic delivery of brimonidine. *Acta Biomater* 2018;**79**:344−53.
33. Giménez-Marqués M, Hidalgo T, Serre C, Horcajada P. Nanostructured metal-organic frameworks and their bio-related applications. *Coord Chem Rev* 2016;**307**:342−60.
34. Smaldone RA, Forgan RS, Furukawa H, Gassensmith JJ, Slawin AMZ, Yaghi OM, et al. Metal-organic frameworks from edible natural products. *Angew Chem Int Ed* 2010;**49**:8630−4.
35. Forgan RS, Smaldone RA, Gassensmith JJ, Furukawa H, Cordes DB, Li QW, et al. Nanoporous carbohydrate metal-organic frameworks. *J Am Chem Soc* 2012;**134**:406−17.
36. Li HY, Lv NN, Li X, Liu BT, Feng J, Ren XH, et al. Composite CD-MOF nanocrystals-containing microspheres for sustained drug delivery. *Nanoscale* 2017;**9**:7454−63.
37. Liu BT, Li HY, Xu XN, Li X, Lv NN, Singh V, et al. Optimized synthesis and crystalline stability of gamma-cyclodextrin metal-organic frameworks for drug adsorption. *Int J Pharm* 2016;**514**:212−9.
38. He YZ, Zhang W, Guo T, Zhang GQ, Qin W, Zhang L, et al. Drug nanoclusters formed in confined nano-cages of CD-MOF: dramatic enhancement of solubility and bioavailability of azilsartan. *Acta Pharm Sin B* 2019;**9**:97−106.
39. Mohtar N, Taylor KMG, Sheikh K, Somavarapu S. Design and development of dry powder sulfobutylether-beta-cyclodextrin complex for pulmonary delivery of fisetin. *Eur J Pharm Biopharm* 2017;**113**:1−10.
40. Kinnarinen T, Jarho P, Jarvinen K, Jarvinen T. Pulmonary deposition of a budesonide/gamma-cyclodextrin complex *in vitro*. *J Control Release* 2003;**90**:197−205.
41. Loftsson T, Jarho P, Masson M, Jarvinen T. Cyclodextrins in drug delivery. *Expet Opin Drug Deliv* 2005;**2**:335−51.
42. Stigliani M, Aquino RP, Del Gaudio P, Mencherini T, Sansone F, Russo P. Non-steroidal anti-inflammatory drug for pulmonary administration: design and investigation of ketoprofen lysinate fine dry powders. *Int J Pharm* 2013;**448**:198−204.
43. Hu J, Liu H, Xu P, Shang Y. Investigation of drug for pulmonary administration-model pulmonary surfactant monolayer interactions using Langmuir-Blodgett monolayer and molecular dynamics simulation: a case study of ketoprofen. *Langmuir* 2019;**35**:13452−60.
44. Singh V, Guo T, Xu HT, Wu L, Gu JK, Wu CB, et al. Moisture resistant and biofriendly CD-MOF nanoparticles obtained *via* cholesterol shielding. *Chem Commun* 2017;**53**:9246−9.
45. Lin L, Quan GL, Peng TT, Huang ZW, Singh V, Lu M, et al. Development of fine solid-crystal suspension with enhanced solubility, stability, and aerosolization performance for dry powder inhalation. *Int J Pharm* 2017;**533**:84−92.
46. Wang SZ, McGuirk CM, d'Aquino A, Mason JA, Mirkin CA. Metal-organic framework nanoparticles. *Adv Mater* 2018;**30**:1800202.
47. Peng TT, Lin SQ, Niu BY, Wang XY, Huang Y, Zhang XJ, et al. Influence of physical properties of carrier on the performance of dry powder inhalers. *Acta Pharm Sin B* 2016;**6**:308−18.
48. Sheng JJ, Kasim NA, Chandrasekharan R, Amidon GL. Solubilization and dissolution of insoluble weak acid, ketoprofen: effects of pH combined with surfactant. *Eur J Pharmaceut Sci* 2006;**29**:306−14.
49. Velaga SP, Djuris J, Cvijic S, Rozou S, Russo P, Colombo G, et al. Dry powder inhalers: an overview of the *in vitro* dissolution methodologies and their correlation with the biopharmaceutical aspects of the drug products. *Eur J Pharmaceut Sci* 2018;**113**:18−28.
50. Marple VA, Roberts DL, Romay FJ, Miller NC, Truman KG, Holroyd MJ, et al. Next generation pharmaceutical impactor (a new impactor for pharmaceutical inhaler testing). Part I: design. *J Aerosol Med-Depos Clear Eff Lung* 2003;**16**:283−99.

51. Hu XX, Wang CF, Wang LB, Liu ZX, Wua L, Zhang GQ, et al. Nanoporous CD-MOF particles with uniform and inhalable size for pulmonary delivery of budesonide. *Int J Pharm* 2019;**564**:153−61.
52. Vanbever R, Mintzes JD, Wang J, Nice J, Chen D, Batycky R, et al. Formulation and physical characterization of large porous particles for inhalation. *Pharm Res* 1999;**16**:1735−42.
53. Zhang XJ, Yue X, Cui YT, Zhao ZY, Huang Y, Cai SH, et al. A systematic safety evaluation of nanoporous mannitol material as a dry-powder inhalation carrier system. *J Pharm Sci* 2020;**109**: 1692−702.
54. Irvin CG, Bates JH. Measuring the lung function in the mouse: the challenge of size. *Respir Res* 2003;**4**:4.
55. Okuda T, Morishita M, Mizutani K, Shibayama A, Okazaki M, Okamoto H. Development of spray-freeze-dried siRNA/PEI powder for inhalation with high aerosol performance and strong pulmonary gene silencing activity. *J Control Release* 2018;**279**:99−113.